Biophysical Chemistry 41 (1991) 253–261
Elsevier Science Publishers B.V., Amsterdam

BIOCHE 01594

Equilibrium and kinetic studies of the binding of tri- and tetra-anionic ligands to bovine serum albumin

Kiyofumi Murakami

Department of Chemistry, Faculty of Education, Yamaguchi University, Yoshida 1677-1, Yamaguchi 753 (Japan)

(Received 21 December 1990; accepted in revised form 10 April 1991)

Abstract

The binding of tri- and tetra-anionic azo dyes (Amaranth, Ponceau 4R, and Ponceau 6R) to bovine serum albumin (BSA) at pH = 7.0 and 25 °C has been studied by equilibrium dialysis, spectrophotometry, and by stopped-flow and temperature-jump methods. Equilibrium dialysis revealed that BSA has one primary binding site and about two secondary sites for each dye. The values of the binding constant for the primary site show that the stability of the complex at the primary site progressively increases with an increase in the number and the density of anionic charges on ligand. Kinetic data have been found to be consistent with a scheme in which a rapid bimolecular binding is followed by two isomerizations of the complex (in the case of Amaranth) or by one isomerization (in the cases of Ponceau 4R and Ponceau 6R). Equilibrium and rate constants for each step of the scheme were determined. From the results it was found that the increment of the number and the density of anionic charges on ligand accelerates the forward process of the final isomerization step but retards the backward one of it, resulting in the enhancement of the stability of the complex at the primary site. On the basis of these results and the structure of the ligands, the detailed binding mechanism has been discussed in the light of the electrostatic interaction between the ligands and the binding site on BSA.

Keywords: Bovine serum albumin; Ligand-binding kinetics; Tri- and tetra-anionic ligands; Isomerization modes; Electrostatic interaction

1. Introduction

A purpose of physicochemical studies of the interaction between serum albumin and ligands is to establish the interrelation between their structures and ligand-binding mechanism of the protein.

Recently, a three-dimensional model structure of albumin molecules has been proposed by Brown [1]. On the basis of the structure and the information about the location of binding sites in the primary sequence of the protein [2–11], nature of the binding sites has been explored [12,13]. Especially, this approach has given a successful insight into the binding of long-chain fatty acids to albumin molecules [12]. On the other hand, kinetic techniques such as stopped-flow [14–22], temperature-jump [23–25], and pressure-jump methods [26,27] have revealed binding schemes. According to the results, the binding of ligands to albumin molecules generally proceeds through the multi-step reaction in which a bimolecular

binding is followed by some isomerizations of the complex (stabilization steps). It is also pointed out that these isomerizations are closely related to those of pure albumin molecules [19,24,25]. In spite of these many investigations, we know too little to predict the binding mechanism for any ligand.

The present paper describes the kinetics and mechanism of the binding of tri- and tetra-anionic ligands (Amaranth, Ponceau 4R, and Ponceau 6R) to bovine serum albumin, which have so far been studied neither from the equilibrium point of view nor the kinetic one, and will show the effects of the number and density of anionic charges on ligand upon the binding mechanism.

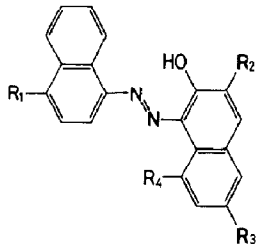

Dye	R_1	R_2	R_3	R_4
Amaranth	SO_3Na	SO_3Na	SO_3Na	H
Ponceau 4R	SO_3Na	H	SO_3Na	SO_3Na
Ponceau 6R	SO_3Na	SO_3Na	SO_3Na	SO_3Na

Fig. 1. Chemical structure of dyes.

2. Materials and methods

2.1 Materials

Bovine serum albumin (Fraction V) purchased from Armour was defatted by means of charcoal treatment in an acid solution [28], lyophilized, and stored at 4 °C. The dimer content of this sample was about 6%, as determined by gel chromatography with TSK G3000SW [1]. The molar concentration of BSA was determined from the absorbance at 280 nm ($E^{1\%}_{1\,cm} = 6.6$ [29]), assuming a molecular weight of 67 kDa. Amaranth, Ponceau 4R and Ponceau 6R were purchased from Tokyo Chemical Industry Co., Ltd., purified by three times recrystallization from an aqueous ethanol solution, and dried at 110 °C for 20 hours. Figure 1 illustrates the chemical structures of the dyes. The pK_a value of the hydroxyl group of these dyes was found to be larger than 10, and no spectral change has been observed over the pH range from 3 to 9. From the concentration dependence of absorption spectrum at pH 7.0, molar extinction coefficients were determined as $\varepsilon_{522} = 2.56 \times 10^4\ M^{-1}\ cm^{-1}$ (Amaranth), $\varepsilon_{507} = 2.49 \times 10^4\ M^{-1}\ cm^{-1}$ (Ponceau 4R) and $\varepsilon_{517} = 2.57 \times 10^4\ M^{-1}\ cm^{-1}$ (Ponceau 6R). All the other chemicals used were reagent-grade. All the sample solutions were prepared in a 0.1 M phosphate buffer of pH = 7.00 ± 0.02.

2.2 Methods

The extent of binding was determined by the use of the equilibrium dialysis technique. Visking dialysis tubing (24/32) cut to a length of 9 cm was treated twice with a 1% $NaHCO_3$ aqueous solution at 100 °C for 40 min and subsequently with a 95% aqueous ethanol solution overnight, soaked in a warm 1% EDTA solution for 30 min, and then exhaustively rinsed with distilled water. A 5 ml sample of the BSA solution ([BSA] = 5×10^{-5} M) placed inside the dialysis tubing was dialyzed against 10 ml of the dye solution at 25 °C for 48 hours. After equilibration, the concentration of the dye solution outside the dialysis tubing was determined spectrophotometrically using the molar-extinction coefficients cited in Section 2.1. The extent of binding was calculated taking into account the amount of adsorbed dye on the dialysis tubing which were determined by a series of blank measurements without BSA.

Spectrophotometric measurements were carried out with Shimadzu UV-200S and UV-100 spectrophotometers.

[1] The gel chromatography measurement also showed that the dimer portion binds the present ligands by the negligible amount, i.e., about 1.5% of the bound dye. It is, therefore, thought that the presence of the dimer does not lead to serious errors.

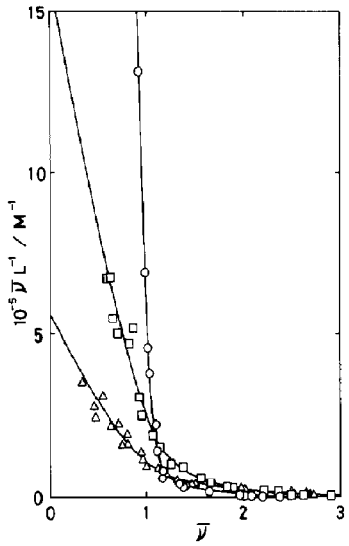

Fig. 2. The Scatchard plots of the interaction between BSA and Amaranth (△), Ponceau 4R (□), and Ponceau 6R (○) at 25 °C and pH = 7.0. The solid lines represent theoretical curves calculated from the values of the binding parameters listed in Table 1.

Temperature-jump measurements were performed with a Unisoku TF-102 fluorescence temperature-jump spectrophotometer. The data were obtained at the temperature-rise of 5 °C. The details of the apparatus have been reported elsewhere [30]. Stopped-flow measurements were carried out using a Union Giken stopped-flow apparatus (RA401) at 1 : 1 mixing ratio. All the experiments were performed at 25 ± 0.2 °C.

All the calculations were accomplished with an Acos-850 computer system (NEC Corporation).

3. Results

3.1 Binding parameters

Figure 2 illustrates the Scatchard plots of the interaction between BSA and Amaranth, Ponceau 4R and Ponceau 6R at pH = 7.0 and 25 °C. These curved plots show that BSA has at least two classes of binding sites for each ligand. Assuming that all the binding sites are independent to each other, the number of moles of the ligand bound per molecule of the protein ($\bar{\nu}$) can be expressed by [31].

Table 1

Binding parameters

Dye	n_1	K_1^* ($10^6\ M^{-1}$)	n_2	K_2^* ($10^4\ M^{-1}$)
Amaranth	0.9	0.6	2.4	1.2
Ponceau 4R	1.0	1.4	1.8	1.8
Ponceau 6R	1.0	9.6	1.4	0.8

$$\bar{\nu} = \frac{n_1 K_1^* L}{1 + K_1^* L} + \frac{n_2 K_2^* L}{1 + K_2^* L} \qquad (1)$$

where n, K^* and L are the number of binding sites, the binding constant and the free ligand concentration, respectively, and the subscripts 1 and 2 refer to the primary and the secondary binding sites. The data were fitted to eq. (1) by a non-linear regression analysis of Nakagawa and Oyanagi [32]. The values of the binding parameters determined are listed in Table 1. As Fig. 2 shows, the observed data fall on the theoretical curves (solid lines) calculated using these values. Table 1 shows that BSA has one strong binding site (primary site) and about two relatively weak sites (secondary sites) for each of the ligands, and that the value of the binding constant for the primary site progressively increases with an increase in the number and the density of anionic charges on the ligand (Amaranth → Ponceau 4R → Ponceau 6R) while that of the secondary sites is unchanged or somewhat reduced.

3.2 Spectrophotometric titration

Figure 3 shows the absorption spectra of Amaranth in the presence of BSA at several concentrations. As can be seen in this figure, the absorbance around 522 nm at which free dye has a maximum absorption decreases but that around 590 nm increases with an increase in the concentration of BSA, showing an approximate isosbestic point at 555 nm. The absorption spectra of Ponceau 4R and Ponceau 6R showed similar changes but such a clear isosbestic point has not been observed. In any case, the fact that the

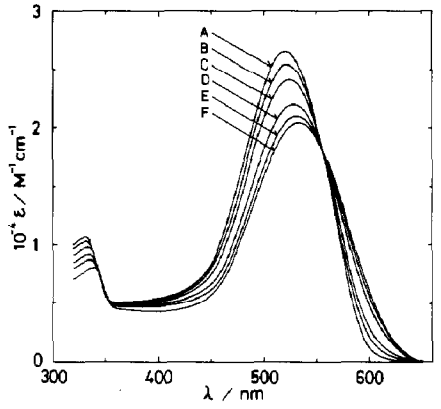

Fig. 3. Absorption spectra of Amaranth in the presence of BSA. The data were obtained at 25 °C, pH = 7.0 and $L_0 = 2.00 \times 10^{-5}$ *M*. (A) Dye only, (B) $P_0/L_0 = 0.2$, (C) $P_0/L_0 = 0.4$, (D) $P_0/L_0 = 1$, (E) $P_0/L_0 = 2$, and (F) $P_0/L_0 = 10$.

binding constants for the primary sites of these dyes are fairly large compared to those for the secondary sites (Table 1) suggests that these spectral changes reflect the bound state at the primary site at least in the region of P_0/L_0 (protein-to-ligand ratio) > 1.

3.3 Kinetic data

From the temperature-jump measurements two distinct relaxation processes have been observed for the BSA–Amaranth sytem (Fig. 4). In the cases of Ponceau 4R and Ponceau 6R, the amplitudes of temperature-jump signals were too small to yield accurate relaxation times. Therefore, kinetic data for these systems were collected through stopped-flow measurements. Figs. 5 and 6 show typical traces observed after the mixing of BSA and Ponceau 4R solutions and that for BSA-Ponceau 6R system, respectively. The wavelengths for the kinetic measurements have been selected so as to give a good signal-to-noise ratio.

The relaxation time (τ) for each process was determined from a semi-logarithmic plot of the trace. Figures 7–9 show P_0/L_0 dependence of the reciprocal relaxation times at $L_0 = 2 \times 10^{-5}$ *M*. To direct our attention to the primary binding site, the data have mainly been collected over the range of $P_0/L_0 \geqq 1$. Figure 7 shows that τ_F^{-1} (fast relaxation) increases with an increase in P_0/L_0

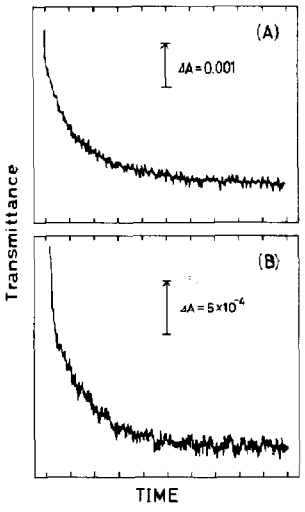

Fig. 4. Typical temperature-jump relaxation curves observed for BSA–Amaranth system at 25 °C, pH = 7.0, $L_0 = 2 \times 10^{-5}$ *M*, and $P_0/L_0 = 4$. (A) $\lambda = 590$ nm, 2 ms per division, (B) $\lambda = 590$ nm, 20 ms per division. The arrow designated for each curve shows the magnitude and the direction of the positive absorbance change.

and reaches a plateau value at high P_0/L_0 values, while τ_S^{-1} (slow relaxation) does not depend on P_0/L_0. These facts suggest that both of the

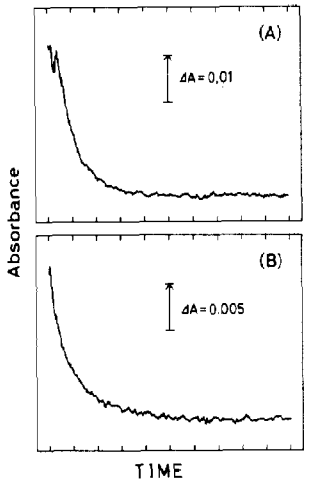

Fig. 5. Typical traces of the absorbance change observed after the mixing of BSA (8×10^{-5} *M*) and Ponceau 4R (4×10^{-5} *M*) solutions at 25 °C. (A) $\lambda = 500$ nm, 5 ms per division, (B) $\lambda = 550$ nm, 25 ms per division. The arrow designated for each trace shows the magnitude and the direction of the positive absorbance change.

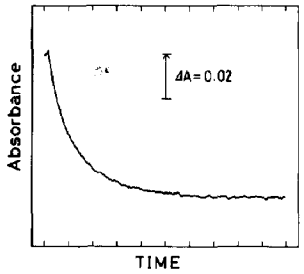

Fig. 6. A typical trace of the absorbance change observed at 520 nm after the mixing of BSA (8×10^{-5} M) and Ponceau 6R (4×10^{-5} M) solutions at 25 °C. The horizontal scale is 25 ms per division. The arrow shows the magnitude and the direction of the positive absorbance change.

two processes observed for BSA–Amaranth system are isomerizations of the complex formed by a rapid bimolecular binding step. Contrary to the case of this system, τ_F^{-1} in Fig. 8 linearly increases with P_0/L_0, while τ_S^{-1} has a tendency to reach a plateau value at high P_0/L_0 values. This behavior suggests that the fast process of the BSA-Ponceau 4R system is a bimolecular binding

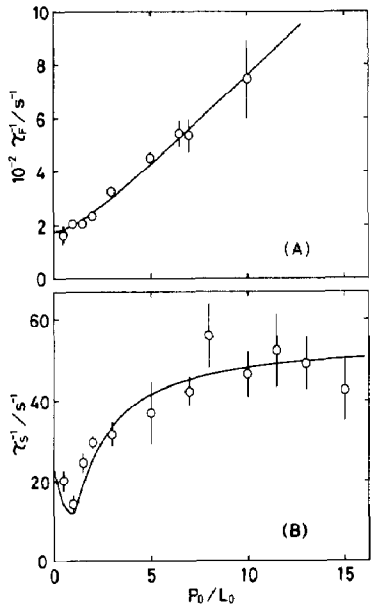

Fig. 8. Plot of τ_F^{-1} (A) and τ_S^{-1} (B) vs. P_0/L_0 for BSA–Ponceau 4R system at $L_0=2\times10^{-5}$ M. The solid lines represent the theoretical curves (eqs. 8 and 9) calculated from the equilibrium and the rate constants listed in Table 2 (see text).

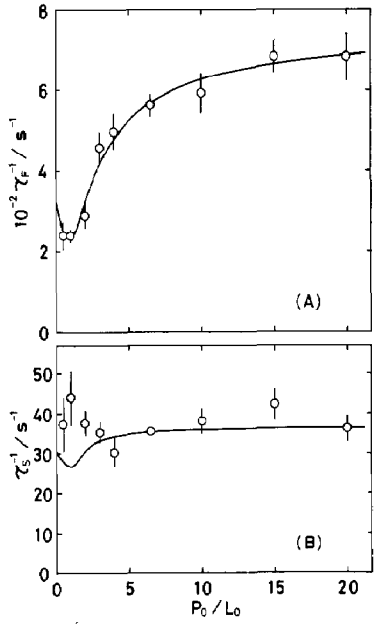

Fig. 7. Plot of τ_F^{-1} (A) and τ_S^{-1} (B) vs. P_0/L_0 for BSA–Amaranth system at $L_0=2\times10^{-5}$ M. The solid lines represent the theoretical curves (eqs. 3 and 4) calculated from the equilibrium and the rate constants listed in Table 2 (see text).

step but the slow one is an isomerization of the complex. In the case of BSA-Ponceau 6R system, the concentration dependence of τ^{-1} (Fig. 9) suggests that the observed process is an isomerization subsequent to a rapid bimolecular binding

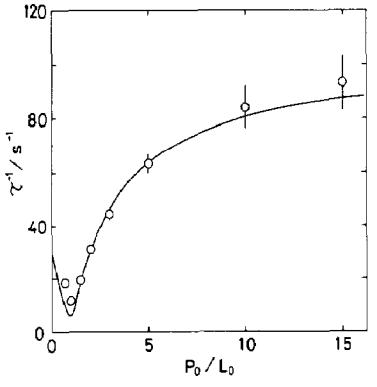

Fig. 9. Plot of τ^{-1} vs. P_0/L_0 for BSA-Ponceau 6R system at $L_0=2\times10^{-5}$ M. The solid line represents the theoretical curve (eq. 9) calculated from the parameters in Table 2 (see text).

step. It should be noted that the relaxation time of the slow process observed for all the ligands lies in the same range of magnitude (τ_S^{-1}: 10–100 s^{-1}).

3.4 Analysis of the kinetic data

3.4.1 BSA–Amaranth system

According to the suggestion derived in the previous section, the kinetic data for the BSA–Amaranth system may be interpreted by the following scheme:

$$P + L \overset{K_1}{\rightleftharpoons} C_1 \underset{k_{-2}}{\overset{k_2}{\rightleftharpoons}} C_2 \underset{k_{-3}}{\overset{k_3}{\rightleftharpoons}} C_3 \qquad (2)$$

where P, L and C_i denote free protein, free ligand and complex species, respectively, and K_i, k_i, and k_{-i} are the equilibrium constant, the forward and backward rate constants of the ith step. The observed two processes correspond to the second and third steps. This scheme predicts reciprocal relaxation times for the isomerization steps as [33]

$$\tau_F^{-1} = k_2 \frac{K_1(P+L)}{1+K_1(P+L)} + k_{-2} \qquad (3)$$

$$\tau_S^{-1} = k_3 \frac{K_1K_2(P+L)}{1+K_1(1+K_2)(P+L)} + k_{-3} \qquad (4)$$

where P and L, respectively, denote the free protein and free ligand concentrations at equilibrium.

Using the values of binding constants determined from the dialysis measurements, equilibrium concentrations P and L for each data point in Fig. 7 were calculated. The data of τ_F^{-1} in Fig. 7 were, at first, fitted to eq. (3) by the non-linear regression analysis, considering K_1, k_2 and k_{-2} as independent parameters. The equilibrium constant of the second step was then calculated as $K_2 = k_2/k_{-2}$. Since τ_{S1}^{-} in Fig. 7 shows poor concentration dependence, it is difficult to determine k_3 and k_{-3} by applying eq. (4) only from the kinetic data. Hence, the data were analyzed as follows. On one hand, the overall association constant for the scheme in eq. (1) must agree with the binding constant for the primary site (Table 1)

$$K_1^* = K_1 + K_1K_2 + K_1K_2K_3 = 6.03 \times 10^5\ M^{-1} \qquad (5)$$

On the other hand, the asymptotic value of τ_S^{-1} in eq. (4) at high P_0/L_0 values becomes

$$k_3K_1K_2/K_1(1+K_2) + k_{-3} = 37\ s^{-1} \qquad (6)$$

Since the values of K_1 and K_2 have already been determined in the analysis of the fast process, k_3 and k_{-3} can be determined by solving the simultanious eqs. (5) and (6). The results are summarized in Table 2, and theoretical curves for τ_F^{-1} and τ_S^{-1} calculated using these values are illustrated in Fig. 7 as the solid curves.

3.4.2 BSA–Ponceau 4R system

According to the previously noted suggestion, the binding scheme for the BSA–Ponceau 4R system may be written as

$$P + L \underset{k_{-1}}{\overset{K_1}{\underset{k_1}{\rightleftharpoons}}} C_1 \underset{k_{-3}}{\overset{K_3}{\underset{k_3}{\rightleftharpoons}}} C_3 \qquad (7)$$

In this scheme, subscript 3, instead of 2, is used to imply that the apparent rate (reciprocal relax-

Table 2

Summary of kinetic results

Dye	K_1 ($10^4\ M^{-1}$)	k_1 ($10^6\ M^{-1}\ s^{-1}$)	k_{-1} (s^{-1})	K_2	k_2 (s^{-1})	k_{-2} (s^{-1})	K_3	k_3 (s^{-1})	k_{-3} (s^{-1})
Amaranth	2.44	–	–	5.96	651	109	2.97	31.0	10.4
Ponceau 4R	3.42	3.54	104	–	–	–	41.1	54.3	1.32
Ponceau 6R	1.95	–	–	–	–	–	491	103	0.21

ation time) of the isomerization step lies in the range: 10–100 s^{-1}; this corresponds to the final isomerization step in the BSA–Amaranth system, which is marked by the same subscript. Reciprocal relaxation times for this scheme become

$$\tau_F^{-1} = k_1(P+L) + k_{-1} \tag{8}$$

$$\tau_S^{-1} = k_3 \frac{K_1(P+L)}{1+K_1(P+L)} + k_{-3} \tag{9}$$

It should be noted that if we apply these equations to the stopped-flow data (Fig. 8), P and L in each equation mean the concentrations at the end of each step.

The data of τ_F^{-1} (Fig. 8A) were fitted to eq. (8) as follows. First, an arbitrary K_1 was chosen to calculate P and L at the end of the first step. Then the best straight-line fit of τ_F^{-1} vs. $(P+L)$ was found to obtain k_1, k_{-1}, and K_1. The procedure was iterated until all the parameters converged. In the analysis of τ_S^{-1}, eq. (9) cannot be directly applied to the data for an accurate estimation of k_3 and k_{-3}, because as can be expected from Fig. 8(B) the asymptotic value at small $(P+L)$ will give a very small value of k_{-3} accompanied with a large error. Hence, the overall binding constant was also used together

$$K_1^* = K_1(1+K_3) = 1.4 \times 10^6\ M^{-1} \tag{10}$$

By the use of K_1^*, eq. (9) is rearranged as

$$\tau_S^{-1} = k_3\left[\frac{K_1(P+L)}{1+K_1(P+L)} + \frac{1}{K_1^*/K_1 - 1}\right] \tag{11}$$

For each of the data point in Fig. 8(B) all the quantity in the brackets in the right-hand side can be estimated, using the results of the previous data analysis. Therefore, we can estimate k_3 from a linear least-squares fit analysis after which k_{-3} was evaluated from

$$k_{-3} = k_3 K_1/(K_1^* - K_1) \tag{12}$$

The results of these analyses are also listed in Table 2. The solid curves in Fig. 8 are the theoretical ones calculated using these values, which are in fair agreement with the experimental data.

3.4.3 BSA–Ponceau 6R system

In this case, the scheme is similar to that for BSA–Ponceau 4R system:

$$P + L \overset{K_1}{\rightleftharpoons} C_1 \underset{k_{-3}}{\overset{k_3}{\rightleftharpoons}} C_3, \tag{13}$$

with the exception, however, that only the isomerization step was observed by the present measurements. With the use of K_1^*, the reciprocal relaxation time for the isomerization step can also be expressed by eq. (11). This was applied to the data (Fig. 9) so as to determine K_1 and k_3 as independent parameters after which k_{-3} was also determined from eq. (12). The results are summarized in Table 2, and the theoretical curve is drawn in Fig. 9.

4. Discussion

In order to understand the nature of the ligand-binding ability of albumin molecules, a great number of binding studies have so far been performed. It may be regarded as the most important conclusion that a stable complex between an organic anion and albumin molecules is, in many cases, formed by both the electrostatic and the hydrophobic interactions [12,34], i.e., the complex is stabilized by a electrostatic bond between charged groups of the ligand and cationic side chains of the protein, and, at the same time, by forming a hydrophobic bond between hydrophobic parts of the ligand and the hydrophobic hole or crevice of albumin molecules. This conclusion has mainly been derived from studies concerning mono-anionic ligands, because many important ligands such as fatty acids and drugs have this form. Furthermore, the correlation between hydrophobicity of ligands and their binding affinity has sometimes been elucidated [35,36]. However, the effect of the number and the density of charges on ligands has not been examined so far. The results of the present study give us a clue to this point.

Table 1 shows that BSA has one primary site for the present ligands (Amaranth, Ponceau 4R and Ponceau 6R). From the similarity of struc-

ture between these ligands, it is reasonable to consider that the primary sites lie in the same region in BSA molecule. Furthermore, the magnitude of the binding constant progressively increases with the increase in the number and the density of anionic charges on the ligands. Since the back-bone structure of these ligands is unique, it may exclusively be concluded that the behavior results from differences in electrostatic interactions between the ligands and the site. Moreover, such a large increase in the binding constant with the number of charges seems to imply that the site consists of more than one cationic residue. In summary, for multi-charged ligands electrostatic contributions play a very important role for binding. However, it should be noted that other contributions such as hydrophobic interactions may also be involved in the total binding energy. These results are consistent with the proposal of Brown and Shockley [12] that the "mouths" of double funnel-shaped domains are the binding sites of drugs, steroids, dyes and other large alicyclic ring structures. The mouth contains the clusters of basic residues and is further able to offer hydrophobic environment to these ligands in its interior. The location of the primary binding site is now being explored.

Using the results summarized in Table 2, we can illustrate the free energy profile of the reaction along the reaction coordinate as pictured in Fig. 10. The magnitude of K_1 takes similar values for the ligands, showing that the degree of stabilization by the bimolecular binding is similar to

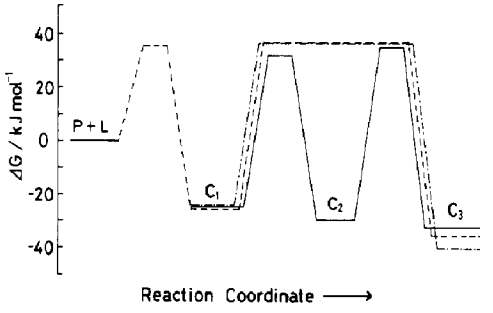

Fig. 10. Free energy profile of the complex formation between BSA and Amaranth (———), Ponceau 4R (- - - - -) and Ponceau 6R (· – · – ·).

each other. The value of k_1 ($3.54 \times 10^6\ M^{-1}\ s^{-1}$) for BSA–Ponceau 4R system suggests that this step is not rate-limited by a diffusion-controlled process [37] but is affected by the steric requirement such as the restricted orientation between the ligand and the binding site. Only from these parameters for the bimolecular binding step, we cannot clearly differentiate between the ligands. However, the clear difference in the reaction scheme, i.e. two isomerizations are involved (eq. 2) for the BSA–Amaranth system whilst only one for the BSA–Ponceau 4R and BSA–Ponceau 6R systems (eqs. 7 and 13), requires us to interpret it in terms of structural difference between the ligands. The differences in the number and the position of sulfonate groups on the ligands must result in different orientations between the ligands and the site in C_1, and consequently may lead to different path-ways to form the final complexes. The formation of the stable intermediate (C_2) for BSA–Amaranth system, which is absent for other systems, may be explained in this way.

One of the most important feauture of the present kinetic results is concerned with the formation of C_3, which is a common step for all the present ligands. Table 2 shows that the value of K_3 progressively increases with an increase in the number and the density of anionic charges on the ligand (in the order of Amaranth → Ponceau 4R → Ponceau 6R). Considering that this tendency agrees with that of K_1^* (Table 1), it may be concluded that the relative stability of the complex at the primary site is mainly determined by the final step. In further details, we can see that the increase of K_3 is achieved by both the increase in k_3 and the decrease in k_{-3} ($K_3 = k_3/k_{-3}$). This means that the more the number and the density of charges on the ligand increase, the sooner C_3 is formed and the longer the life-time of it becomes. Judging from the above mentioned tendencies for the equilibrium and rate constants, the final step may be interpreted as the formation of the residual electrostatic bonds, which is not accomplished by the previous steps. Of course this step must accompany spatial rearrangements of the protein conformation at least in the vicinity of the site.

Scheider [19], Murakami et al. [24] and Murakami [25] have pointed out the possibility that the stabilization steps of albumin–ligand complexes are closely related to some isomerization modes of pure albumin molecules. Murakami [25] has classified the isomerizations in four categories, according to their rate, as mode A (10^3–10^4 s^{-1}), mode B (10^2–10^3 s^{-1}), mode C (10–10^2 s^{-1}) and mode D (1–10 s^{-1}). According to this classification, the final steps of the present schemes (in eqs. 2, 7 and 13) belong to mode C and the second step for BSA–Amaranth system (eq. 2) to mode B. Excepting that modes C and D are related to $N \rightleftharpoons B$ transition of albumin molecules [38] and mode D may accompany a change in the helix content of the protein [39], little is known about the detailed nature of these modes. The results of the present kinetic study, however, may add another characteristic to mode C that it involves spacial rearrangements of the basic residues at the surface of the protein.

References

1 J.R. Brown, in: Albumin structure, function and uses, eds. V.M. Rosenoer, M. Oratz and M.A. Rothschild (Pergamon Press, New York, NY, 1977) p. 27.
2 R.G. Reed, R.C. Feldhoff, O.L. Clute and T. Peters, Jr., Biochemistry 14 (1975) 4578.
3 T.P. King, Arch. Biochem. Biophys. 156 (1973) 509.
4 T. Peters, Jr. and R.C. Feldhoff, Biochemistry 14 (1975) 3384.
5 Z. Hrkal, M. Kodicek, Z. Vodrazka, B. Meloun and L. Moravek, Int. J. Biochem. 9 (1978) 349.
6 T. Sjodin, R. Hansson and I. Sjoholm, Biochim. Biophys. Acta 494 (1977) 61.
7 I. Sjoholm and I. Ljungstedt, J. Biol. Chem. 248 (1973) 8434.
8 K.J. Fehske, W.E. Muller and U. Wollert, Biochem. Pharmacol. 30 (1981) 681.
9 J.E. Walker, FEBS Lett. 66 (1976) 173.
10 J.A. Anderson, H.W. Chang and C.J. Grandjean, Biochemistry 10 (1971) 2408.
11 W.H. Pearlman and I.F.F. Fong, J. Biol. Chem. 247 (1972) 8078.
12 J.R. Brown and P. Shockley, in: Lipid–protein interactions, vol. 1, eds. P.C. Jost and O.H. Griffith (Wiley, New York, NY, 1982) p. 25.
13 U. Kragh-Hansen, Pharmacol. Rev. 33 (1981) 17.
14 R.F. Chen, Arch. Biochem. Biophys. 160 (1974) 106.
15 T. Faerch and J. Jacobsen, Arch. Biochem. Biophys. 184 (1977) 282.
16 R.G. Reed, J. Biol. Chem. 252 (1977) 7483.
17 R.D. Gray and S.D. Stroupe, J. Biol. Chem. 253 (1978) 4370.
18 W. Scheider, Proc. Natl. Acad. Sci. USA 76 (1979) 2283.
19 W. Scheider, J. Phys. Chem. 84 (1980) 925.
20 N. Rietbrock and A. Labmann, Naunyn-Schmiedederg's Arch. Pharmacol. 313 (1980) 269.
21 P.A. Adams and M.C. Berman, Biochem. J. 191 (1980) 95.
22 K. Murakami, Y. Kubota, Y. Fujisaki and T. Sano, Bull. Chem. Soc. Jpn. 59 (1986) 3399.
23 A. Froese, A.H. Sehon and M. Eigen, Can. J. Chem. 40 (1962) 1786.
24 K. Murakami, T. Sano, S. Tsuchie and T. Yasunaga, Biophys. Chem. 21 (1985) 127.
25 K. Murakami, Bull. Chem. Soc. Jpn. 61 (1988) 1323.
26 D.E. Goldsack and P.M. Wearn, Can. J. Biochem. 49 (1971) 1267.
27 K. Murakami, T. Sano and T. Yasunaga, Bull. Chem. Soc. Jpn. 54 (1981) 862.
28 R.F. Chen, J. Biol. Chem. 242 (1967) 173.
29 E.J. Cohn, W.L. Huges, Jr. and J.H. Weare, J. Am. Chem. Soc. 69 (1947) 1753.
30 K. Murakami, K. Mizuguchi, Y. Kubota and Y. Fujisaki, Bull. Chem. Soc. Jpn. 59 (1986) 3393.
31 J. Steinhardt and J.A. Reynolds, Multiple equilibria in proteins (Academic Press, New York, NY, 1969) p. 15.
32 T. Nakagawa and Y. Oyanagi, in: Recent developments in statistical inference and data analysis, ed. K. Matusita (North Holland, New York, NY, 1980) p. 221.
33 C.F. Bernasconi, Relaxation kinetics (Academic Press, New York, NY, 1976) p. 43.
34 E.M. Sellers and J.-K. Weser, in: Albumin structure, function and uses, eds. V.M. Rosenoer, M. Oratz and M.A. Rothschild (Pergamon Press, New York, NY, 1977) p. 159.
35 F. Helmer, K. Kiehs and C. Hansch, Biochemistry 7 (1968) 2858.
36 P.-L. Hsu, J.K.H. Ma, H.W. Jun and L.A. Luzzi, J. Pharm. Sci. 63 (1974) 27.
37 P. Regenfuss and R.M. Clegg, Biophys. Chem. 26 (1987) 83.
38 K. Kuwajima, T. Matsushima, K. Nitta and S. Sugai, Biopolymers 23 (1984) 1347.
39 B. Gruenewald and W. Knoche, Rev. Sci. Instrum. 49 (1978) 797.